Characteristics of energy storage and dissipation in TiNi shape memory alloy

2005 Sci. Technol. Adv. Mater. 6 889

(http://iopscience.iop.org/1468-6996/6/8/A04)

ELSEVIER

Science and Technology of Advanced Materials 6 (2005) 889–894

SCIENCE AND TECHNOLOGY OF ADVANCED MATERIALS

www.elsevier.com/locate/stam

Characteristics of energy storage and dissipation in TiNi shape memory alloy

E. Pieczyska [a,1], S. Gadaj [a], W.K. Nowacki [a], K. Hoshio [b], Y. Makino [b], H. Tobushi [b,*]

[a] *Institute of Fundamental Technological Research, Polish Academy of Sciences, Swietokrzyska 21, Warsaw 00-049, Poland*
[b] *Department of Mechanical Engineering, Aichi Institute of Technology, 1247 Yachigusa, Yakusa-cho, Toyota 470-0392, Japan*

Received 4 March 2005; received in revised form 22 July 2005; accepted 25 July 2005
Available online 2 November 2005

Abstract

The characteristics of energy storage and dissipation in TiNi shape memory alloys were investigated experimentally based on the superelastic properties under various thermomechanical loading conditions. The influence of strain rate, cyclic loading and temperature-controlled condition on the characteristics of energy storage and dissipation of the material was investigated. Temperature on the surface of the material was observed and the influence of variation in temperature on the characteristics was clarified. The results obtained can be summarized as follows. (1) In the case of low strain rate, the stress plateaus appear on the stress-strain curves due to the martensitic transformation and the reverse transformation during loading and unloading. In the case of high strain rate, the slopes of the stress–strain curves are steep in the phase-transformation regions during loading and unloading. The recoverable strain energy per unit volume increases in proportion to temperature, but the dissipated work per unit volume depends slightly on temperature. In the case of low strain rate, the recoverable strain energy and dissipated work do not depend on both strain rate and the temperature-controlled condition. (2) In the case of high strain rate, while the recoverable strain energy density decreases and dissipated work density increases in proportion to strain rate under the temperature-controlled condition, the recoverable strain energy density increases and dissipated work density decreases under the temperature-uncontrolled condition. In the case of the temperature-uncontrolled condition, temperature varies significantly due to the martensitic transformation and therefore the characteristics of energy storage and dissipation differ from these under the temperature-controlled condition. (3) In the case of cyclic loading, both the recoverable strain energy and dissipated work decrease in the early 20 cycles, but change slightly thereafter. (4) The influence of strain rate, cyclic loading and the environment on the characteristics of energy storage and dissipation is important to be considered in the design of shape memory alloy elements.

Keywords: Shape memory ally; Superelasticity; Energy storage; Energy dissipation; Damping; Strain rate; Cyclic deformation; Titanium–nickel alloy; Environment

1. Introduction

The shape memory alloys (SMAs) have been developed as the intelligent materials [1–5]. In SMAs, not only shape memory effect (SME) but also superelasticity (SE) appears. The large strain up to 8% disappears by heating in the case of the SME and by unloading in the case of the SE. The stress plateau appears due to the martensitic transformation (MT) and the reverse transformation during loading and unloading, respectively. In the case of the SE, the large hysteresis loop is observed in the stress–strain curve during loading and unloading. The area surrounded by the hysteresis loop denotes the dissipated work per unit volume. This means the fact that the dissipated work density due to the SE of SMA is high and therefore SMA has high performance of energy absorption or damping for vibration and impact deformation.

On the other hands, in the case of the SE, large strain is recovered by unloading. The area below the unloading curve on the stress–strain diagram represents the recoverable strain-energy density. The stress plateau due to the reverse transformation is high. This means the fact that the recoverable strain–energy density due to the SE of SMA is high and therefore SMA has high performance of energy storage to obtain the mechanical work.

In the recent research, it has been found that the properties of the SE depend on cyclic loading [6–8], strain rate [9–12] and the loading conditions [13–15]. In order to design SMA elements in

* Corresponding author. Tel.: +81 565 48 8121; fax: +81 565 48 4555.
E-mail addresses: epiecz@ippt.gov.pl (E. Pieczyska), tobushi@aitech.ac.jp (H. Tobushi).
[1] Tel.: +48 22 826 12 81; fax: +48 22 826 98 15.

1468-6996/$ - see front matter © 2005 Elsevier Ltd. All rights reserved.
doi:10.1016/j.stam.2005.07.008

which the properties of energy storage and dissipation due to the SE are used, it is important to evaluate these properties properly and to take them into account of the design.

In the present study, the characteristics of energy storage and dissipation in TiNi SMAs were investigated experimentally. The experiments were carried out to investigate the influence of cyclic loading, temperature, strain rate and the temperature-controlled condition on dissipated work density and recoverable strain-energy density. It was confirmed that the characteristics of energy storage and dissipation in SMA depend on the thermomechanical loading condition and therefore these properties are important to be taken into account for the design of SMA elements.

2. Experimental method

2.1. Materials and specimen

The materials used in the experiment were a TiNi SMA wire and a TiNi SMA ribbon which were produced by Furukawa Electric Co., Ltd. Diameter of the wire was 0.75 mm. Width and thickness of the ribbon were 10 and 0.4 mm, respectively. The memorized shape is a straight line for the wire and a flat plane for the ribbon. The reverse-transformation finish temperatures A_f were 323 K for the wire and 277 K for the ribbon. The length and gauge length of the specimen were 100 and 20 mm for wire, and 160 and 100 mm for the ribbon, respectively.

2.2. Experimental apparatus

The SMA characteristic testing machine was used for the experiments for the wire [16]. In the tests, temperature on the surface of the wire was measured through a thermocouple with diameter of 0.1 mm. The temperature was controlled by using the temperature-control system. In this system, specimen was heated by compressed hot air and cooled by liquefied carbon dioxide.

In the experiments for the ribbon, the infrared thermovision camera was used to measure temperature on the surface of the ribbon [17]. In the tests, ambient temperature was room temperature and temperature was not controlled.

2.3. Experimental procedure

In order to investigate the characteristics of energy storage and dissipation of the material, the following four kinds of tension test were carried out. In all tests, uniaxial tensile load was applied to the specimen under various thermomechanical conditions.

(1) Exp. 1: Low-strain rate test

The SMA wire was subjected to uniaxial tensile load under low strain rate of $1.67\times10^{-4}\ s^{-1}$ at constant temperature T. Temperatures were 303, 333, 353, 373 and 393 K. The temperature on the surface of the wire was controlled to keep constant during loading and unloading.

(2) Exp. 2: Cyclic loading test

The SMA wire was subjected to cyclic tensile load at constant temperature T. In each cycle, axial load was applied to maximum strain and perfectly removed thereafter.

(3) Exp. 3: Strain rate test

The SMA wire was subjected to tensile load under various strain rates at constant temperature. In each test, strain rate and temperature were controlled to keep constant. Strain rate was set in the region between $1.67\times10^{-5}\ s^{-1}$ and $1.67\times10^{-2}\ s^{-1}$.

(4) Exp. 4: Temperature-uncontrolled test

The SMA ribbon was subjected to tensile load under various strain rates at room temperature (RT). In the test, ambient temperature at RT was not controlled. The temperature on the surface of the specimen was measured through a thermovision camera.

3. Experimental results and discussion

3.1. Energy storage and dissipation under low-strain rate

The stress-strain curves obtained by the low-strain rate test (Exp. 1) for maximum strain of 7.8% under strain rate $d\varepsilon/dt = 1.67\times10^{-4}\ s^{-1}$ at various temperatures T are shown in Fig. 1. The stress-strain curves for maximum strain of 4% at 353 K are shown in Fig. 2. As can be seen in Fig. 1, the upper stress plateau appears during loading between the points S_M and F_M. If temperature T is higher than $A_f = 323$ K, the lower stress plateau appears during unloading between the points S_A and F_A, and the curve draws a hysteresis loop during loading and unloading, showing the property of the SE. The upper stress plateau appears due to the MT and the lower stress plateau due to the reverse transformation. Both the upper and lower stress plateaus increase with increasing T.

The SE stress–strain diagram is schematically shown in Fig. 3. The area under the loading curve denotes the work per unit volume done during loading. Therefore, the area under the unloading curve denotes the recoverable strain energy per unit

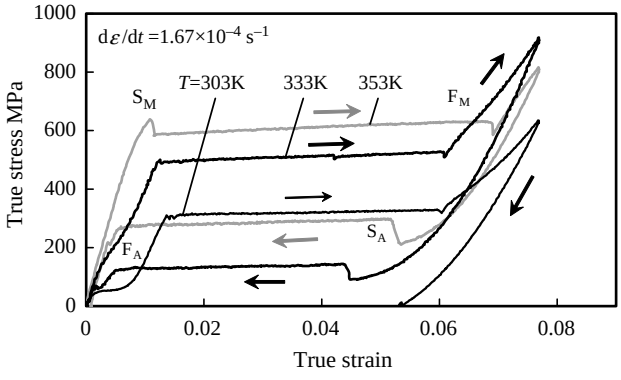

Fig. 1. Stress–strain curves at various temperatures.

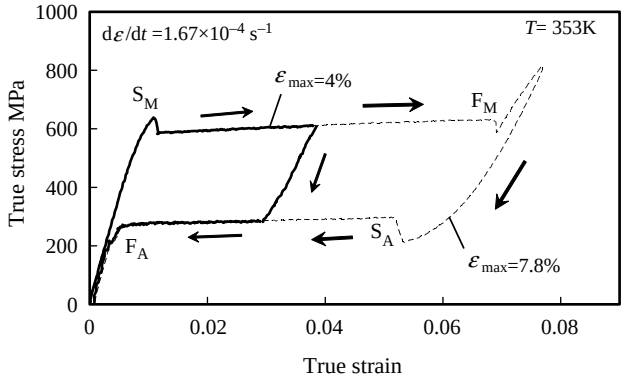

Fig. 2. Stress–strain curves for internal loop loading.

volume E_r. The area inside the hysteresis loop during loading and unloading denotes the dissipated work per unit volume W_d.

The relationships between E_r and W_d and temperature T obtained by the test in which the maximum strain ε_{max} was the MT-finish strain ε_{Mf} are shown in Fig. 4. As can be seen in Fig. 4, E_r and W_d increase with increasing T. The amount of variation in E_r with T at temperatures above A_f is very large, but that in W_d is small. The values of E_r and W_d can be estimated approximately as follows. The stress plateaus due to the MT and the reverse transformation are represented by σ_M and σ_A, respectively, as shown in Fig. 3. The relationships between σ_M and σ_A and temperature T are expressed by the straight lines as follows which are called the transformation lines [18,19].

$$\sigma_M = C_M(T - T_M) \tag{1}$$

$$\sigma_A = C_A(T - T_A) \tag{2}$$

where C_M and C_A represent the slopes of the transformation lines for the MT and the reverse transformation, respectively. T_M and T_A denote the transformation temperatures under no load for the MT and the reverse transformation, respectively.

As shown in Fig. 3, E_r and W_d are estimated approximately by the parallelograms and a triangle as follows.

$$E_r = \sigma_A(\varepsilon_{max} - \varepsilon_{MS}) + \frac{\sigma_M^2}{2E} \tag{3}$$

$$W_d = (\sigma_M - \sigma_A)(\varepsilon_{max} - \varepsilon_{MS}) \tag{4}$$

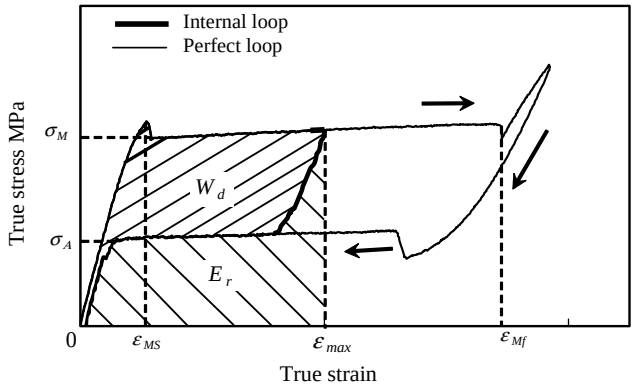

Fig. 3. Schematical superelastic stress-strain diagram showing E_r and W_d.

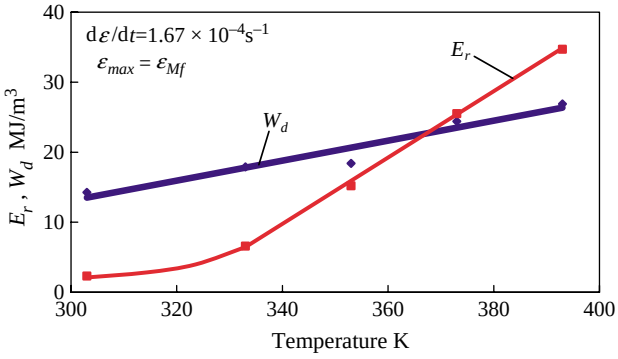

Fig. 4. Dependence of E_r and W_d on temperature.

where ε_{max} and ε_{MS} represent the maximum strain in the internal loop and the MT-start strain, respectively. E denotes modulus of elasticity. In the case of the perfect loop, ε_{max} is equal to the MT-finish strain ε_{Mf}. For TiNi SMA, C_A and C_M take the close values of 5–6 MPa/K. Therefore by assuming $C_A = C_M$ and by using Eqs. (1)–(4), E_r and W_d are expressed as follows.

$$E_r = C_A(T - T_A)(\varepsilon_{max} - \varepsilon_{MS}) + \frac{\{C_A(T - T_M)\}^2}{2E} \tag{5}$$

$$W_d = C_A(T_A - T_M)(\varepsilon_{max} - \varepsilon_{MS}) \tag{6}$$

The dependence of E_r and W_d on T shown in Fig. 4 can be evaluated by Eqs. (5) and (6). Let us calculate E_r and W_d in the case of the perfect loop with $\varepsilon_{max} = \varepsilon_{Mf}$ at $T = 353$ K. If $C_A = 6$ MPa/K, $\varepsilon_{Mf} = 0.07$, $\varepsilon_{MS} = 0.01$, $T_A = 320$ K, $T_M = 260$ K and $E = 80$ GPa for TiNi SMA, the calculated values of E_r and W_d are 14 MJ/m^3 and 21.6 MJ/m^3, respectively. These values are close to the experimental data at 353 K. In the TiNi SMA, while ε_{MS} is 0.01–0.012 and depends slightly on T, ε_{Mf} increases in proportion to T. Therefore, if we evaluate E_r and W_d for the perfect loop by Eqs. (5) and (6), the dependence of ε_{Mf} on T is necessary to be considered.

In conclusion it can be ascertained the fact that E_r and W_d increase in proportion to ε_{max} and that E_r increases with increasing T but W_d depends slightly on T.

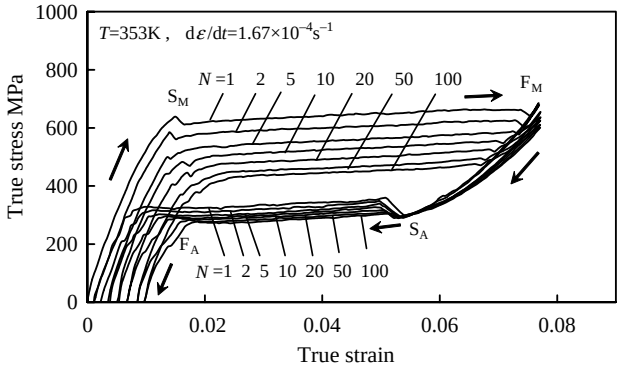

Fig. 5. Stress–strain curves under cyclic loading.

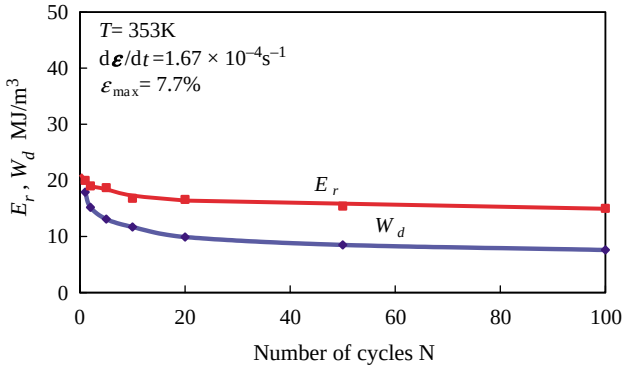

Fig. 6. Dependence of E_r and W_d on number of cycles.

3.2. Energy storage and dissipation under cyclic loading

The stress–strain curves obtained by the cyclic loading test (Exp. 2) for maximum strain of 7.7% and strain rate of $1.67\times10^{-4}\ s^{-1}$ at $T=353$ K are shown in Fig. 5. In the figure, N denotes the number of cycles. The relationships between E_r and W_d and the number of cycles N are shown in Fig. 6. As can be seen in Fig. 5, the upper stress plateau σ_M decreases significantly in the early 20 cycles but decreases gradually thereafter. The lower stress plateau σ_A decreases with an increase in N but the amount of decrease is small.

As can be seen in Fig. 6, both E_r and W_d decrease significantly in the early 20 cycles but approach a certain values thereafter. Therefore, in applications of SMA elements, if mechanical training is used before the practical use, the constant cyclic properties of E_r and W_d can be obtained.

In the case of elastic deformation in normal metals, the relationship between stress and strain obeys the Hooke's law. Therefore, recoverable strain energy E_r can be evaluated as follows.

$$E_r = \frac{\sigma_Y^2}{2E} \tag{7}$$

where σ_Y denotes yield stress. If $E=200$ GPa and $\sigma_Y=200$ MPa for mild steel, $E_r=0.1$ MJ/m^3. Compared with this value, the value of E_r shown in Fig. 6 is about 150 times larger than that of mild steel. This means the fact that the performance of the SE in SMA is excellent as the energy storage material.

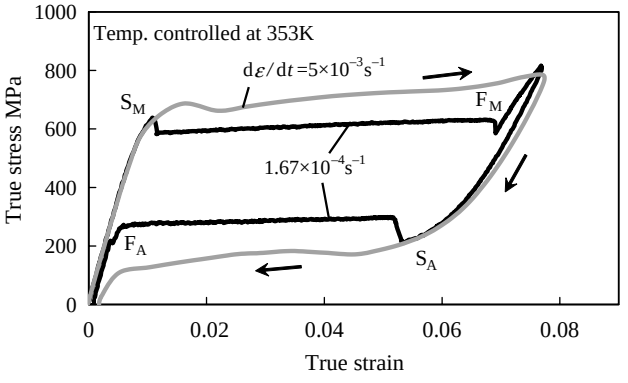

Fig. 7. Stress–strain curves at various strain rates under temperature-controlled condition.

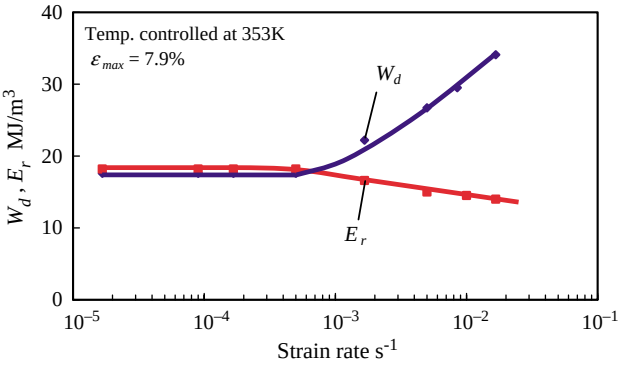

Fig. 8. Dependence of E_r and W_d on strain rate under temperature-controlled condition.

3.3. Energy storage and dissipation under various strain rates

The stress-strain curves obtained by the strain rate test (Exp. 3) for maximum strain of 7.9% at $T=353$ K under strain rates $d\varepsilon/dt=1.67\times10^{-4}\ s^{-1}$ and $5\times10^{-3}\ s^{-1}$ are shown in Fig. 7. The relationships between E_r and W_d and strain rate $d\varepsilon/dt$ for $\varepsilon_{max}=7.9\%$ are shown in Fig. 8.

As can be seen in Fig. 7, in the case of $d\varepsilon/dt=1.67\times10^{-4}\ s^{-1}$, an overshoot appears at the MT-start point S_M followed by the upper stress plateau to the finish point F_M in the loading process. In the same manner, an undershoot appeases at the start point S_A of the reverse transformation followed by the lower stress plateau to the finish point F_A in the unloading process. On the other hand, in the case of $d\varepsilon/dt=5\times10^{-3}\ s^{-1}$, the overshoot, undershoot and clear stress plateau do not appear. The slope of the stress–strain curve is steep in the regions of the MT and the reverse transformation.

As can be seen in Fig. 8, E_r and W_d are constant in the region of strain rate below $d\varepsilon/dt=5\times10^{-4}\ s^{-1}$. E_r decreases and W_d increases in proportion to strain rate in the region of strain rate above $d\varepsilon/dt=5\times10^{-4}\ s^{-1}$. Therefore, it is ascertained that, in the case of higher strain rate, the function of energy storage is lower but that of energy dissipation or absorption is higher.

3.4. Deformation properties under temperature-uncontrolled condition

The stress-strain curves obtained by the temperature-uncontrolled test (Exp. 4) under strain rates $d\varepsilon/dt=5\times10^{-4}\ s^{-1}$ and $10^{-1}\ s^{-1}$ are shown in Fig. 9. The stress-strain curve and the variation in temperature for $d\varepsilon/dt=10^{-2}\ s^{-1}$ during loading and unloading are shown in Fig. 10. In the test, the ambient temperature was room temperature and temperature was not controlled. Temperature on the surface of the specimen was measured through the thermovision camera. Temperature increases based on the MT. At the point S_M, the thin transformation band inclined by 42° to the axial direction of the specimen under tension appears in the central part of the specimen [17]. The transformation band in which temperature is high expands with progress of the MT. In Fig. 10, the variation in temperature ΔT_p denotes the value at the position where the transformation band appeared at first. The variation in

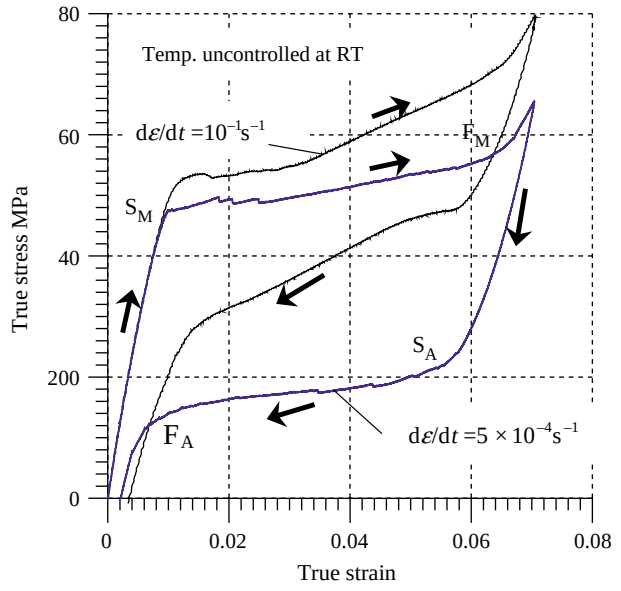

Fig. 9. Stress–strain curves at various strain rates under temperature-uncontrolled condition.

temperature ΔT was obtained as an average value of temperature variation on the surface area (10 mm × 100 mm) of the specimen.

As can be seen in Fig. 9, the upper stress plateau and the lower stress plateau appear in the case of $d\varepsilon/dt = 5 \times 10^{-4}\ s^{-1}$ during loading and unloading. On the other hand, in the case of $d\varepsilon/dt = 10^{-1}\ s^{-1}$, the slopes of the stress-strain curves are steep in the regions of the MT and the reverse transformation.

As can be seen in Fig. 10, temperature variation ΔT increases up to 28 K due to the MT during loading. At the start point S_A of the reverse transformation, temperature is still higher than room temperature by about 25 K. In this test, temperature was not controlled to keep constant, and therefore heat generated due to the MT is difficult to be transfered into air in a short time under high strain rate and the amount of decrease in temperature ΔT at the point S_A is small. Between the start point S_A and the finish

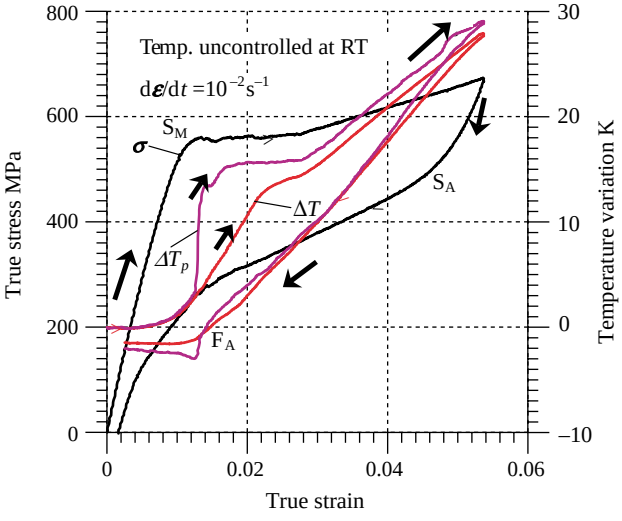

Fig. 10. Stress–strain curve and variation in temperature during loading and unloading at strain rate of $10^{-2}\ s^{-1}$ under temperature-uncontrolled condition.

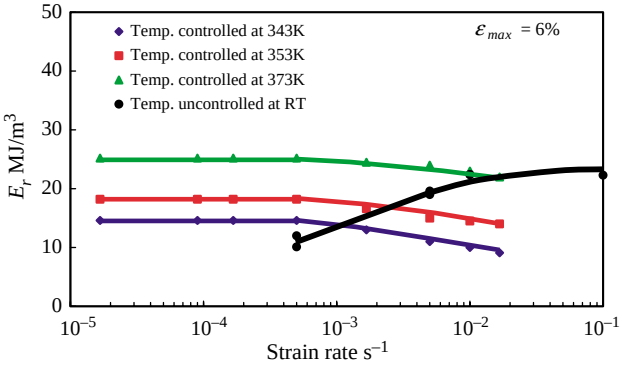

Fig. 11. Dependence of E_r on strain rate under temperature-controlled and -uncontrolled conditions.

point F_A of the reverse transformation, the reverse transformation progresses and temperature decreases due to the reverse transformation. Since the transformation stress increases with increasing temperature as expressed by Eqs. (1) and (2), the slope of the stress-strain curve is steep according to an increase in temperature due to the MT in the loading process. In the same manner, the slope is also steep according to a decrease in temperature due to the reverse transformation in the unloading process. Since the reverse transformation occurs under high stress due to high temperature at the point S_A, the slope of the unloading curve is steeper.

3.5. Influence of temperature-controlled condition on energy storage and dissipation

The relationships between recoverable strain energy density E_r and strain rate $d\varepsilon/dt$ for maximum strain of 6% in the case of temperature-controlled condition (Exp. 3) and the temperature-uncontrolled condition (Exp. 4) are shown in Fig. 11. Also the relationships between dissipated work density W_d and $d\varepsilon/dt$ are shown in Fig. 12.

As can be seen in Figs. 11 and 12, both E_r and W_d are constant in the region of low strain rate below $d\varepsilon/dt = 5 \times 10^{-4}\ s^{-1}$. In the region of higher strain rate above $d\varepsilon/dt = 5 \times 10^{-4}\ s^{-1}$, while E_r decreases and W_d increases in proportion to strain rate in the case of temperature-controlled condition, E_r increases and W_d decreases in the case of temperature-uncontrolled condition.

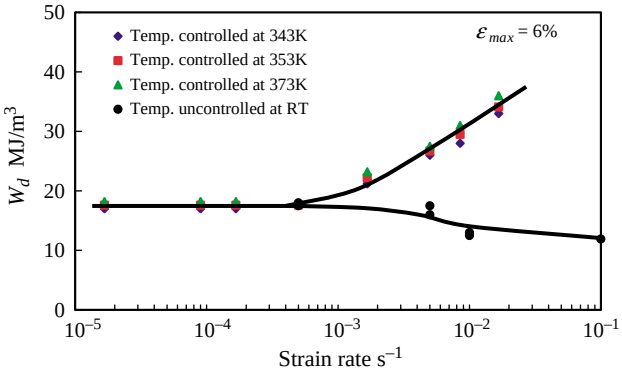

Fig. 12. Dependence of W_d on strain rate under temperature-controlled and -uncontrolled conditions.

As discussed in the previous section, in the case of temperature-uncontrolled condition under high strain rate, there is not enough time for heat generated due to the MT to be transfered into air, and therefore temperature varies significantly, resulting in large variation in stress. Based on large variation in stress, E_r increases and W_d decreases under high strain rate. The condition under low strain rate corresponds to the isothermal process and the condition under high strain rate to the adiabatic process.

In applications of SMA elements, the temperature-uncontrolled condition corresponds to the case to be used in air without airflow. The temperature-controlled condition corresponds to the case for thin SMA elements subjected to airflow at high velocity or used in water. The dependence of E_r and W_d on strain rate under high strain rate is quite different between the temperature-controlled and temperature-uncontrolled conditions. Therefore, it is important to consider the influence of the environment or the temperature-controlled condition on energy storage and dissipation under high strain rate in the design of SMA elements.

4. Conclusions

The characteristics of energy storage and dissipation in TiNi shape memory alloys were investigated based on the superelastic properties under various thermomechanical loading conditions. The results obtained can be summarized as follows.

(1) In the case of low strain rate, the stress plateau appears due to the martensitic transformation and the reverse transformation during loading and unloading. In the case of high strain rate, the slopes of the stress – strain curves are steep in the phase-transformation regions during loading and unloading. The recoverable strain energy increases in proportion to temperature, but the dissipated work depends slightly on temperature. In the case of low strain rate, the recoverable strain energy and dissipated work do not depend on both strain rate and the temperature-controlled condition.
(2) In the case of high strain rate, while the recoverable strain energy decreases and dissipated work increases in proportion to strain rate under the temperature-controlled condition, the recoverable strain energy increases and the dissipated work decreases under the temperature-uncontrolled condition.
(3) In the case of cyclic loading, both the recoverable strain energy and dissipated work decrease in the early 20 cycles, but change slightly thereafter.
(4) It is important for the design of SMA elements to take account of the influence of strain rate, cyclic loading and the environment on the characteristics of energy storage and dissipation.

Acknowledgements

The experimental work of this study was carried out with the assistance of the students of Aichi Institute of Technology, to whom the authors wish to express their gratitude. The authors also wish to extend their thanks to the Polish Academy of Science (PAS) and the Japan Society for the Promotion of Science (JSPS) for financial support. This study was performed in the course of the program in the Bilateral Joint Research Project between Institute of Fundamental Technological Research and Aichi Institute of Technology supported by PAS and JSPS.

References

[1] H. Funakubo (Ed.), Shape Memory Alloys, Gordon and Breach, New York, 1998.
[2] T.W. Duering, K.N. Melton, D. Stockel, C.M. Wayman (Eds.), Engineering Aspects of Shape Memory Alloys, Butterworth-Heinemann, London, 1990.
[3] K. Otsuka, C.M. Wayman (Eds.), Shape Memory Materials, Cambridge University Press, Cambridge, 1998.
[4] T. Saburo (Ed.), Shape Memory Materials, Trans Tech Publications, Hardcover, 2000.
[5] Y.Y. Chu, L.C. Zhao (Eds.), Shape Memory Materials and its Applications, Trans Tech Publications, Hardcover, 2002.
[6] S. Miyazaki, T. Imai, Y. Igo, K. Otsuka, Effect of cyclic deformation on the pseudoelasticity characteristics of Ti–Ni alloys, Met. Trans. A 17 (1986) 115–120.
[7] S. Miyazaki, Thermal and Stress Cycling Effects and Fatigue Properties of Ti–Ni Alloys, Butterworth-Heinemann, London, 1990, pp. 394–413.
[8] J.M. Gong, H. Tobushi, K. Takata, K. Okumura, Superelastic deformation of a TiNi shape memory alloy subjected to various cyclic loadings, Proc. Instn. Mech. Eng. Part L: J. Mater.: Des. Appl. 216 (2002) 17–23.
[9] J.A. Shaw, S. Kyriakides, Thermomechanical aspects of NiTi, J. Mech. Phys. Solids 43 (8) (1995) 1243–1281.
[10] D. Wolons, F. Gandhi, B. Malovrh, Experimental investigation of the pseudoelastic hysteresis damping characteristics of shape memory alloy wires, J. Intell. Mater. Syst. Struct. 9 (1998) 116–126.
[11] S.P. Gadaj, W.K. Nowacki, H. Tobushi, Temperature evolution during tensile test of TiNi shape memory alloy, Arch. Mech. 51 (6) (1999) 649–663.
[12] H. Tobushi, K. Takata, Y. Shimeno, W.K. Nowack, S.P. Gadaj, Influence of strain rate on superelastic behaviour of TiNi shape memory alloy, Proc. Instn. Mech. Eng. Part L 213 (1999) 93–102.
[13] G. Socha, B. Raniecki, S. Miyazaki, Influence of control parameters on inhomogeneity and the deformation behavior of Ti-51.0at%Ni SMA undergoing martensitic phase transformation at pure tension, 33rd Solids Mechanics Conference, 2000, pp. 369–370.
[14] H. Tobushi, K. Okumura, M. Endo, K. Tanaka, Deformation behavior of TiNi shape-memory alloy under strain- or stress-controlled conditions, Arch. Mech. 54 (1) (2002) 75–91.
[15] R. Matsui, H. Tobushi, T. Ikawa, Transformation-induced creep and stress relaxation of TiNi shape memory alloy, Proc. Instn. Mech. Eng. Part L: J. Mater.: Des. Appl. 218 (2004) 343–353.
[16] H. Tobushi, K. Tanaka, K. Kimura, T. Hori, T. Sawada, Stress–strain–temperature relationship associated with the R-phase transformation in TiNi shape memory alloy, JSME Inter. J., Ser. I 35 (3) (1992) 278–284.
[17] E. Pieczyska, S. Gadaj, W. Nowacki, H. Tobushi, Investigation of nucleation and propagation of phase transformation in TiNi SMA, QIRT J. 1 (1) (2004) 117–127.
[18] K. Tanaka, A thermomechanical sketch of shape memory effect: one-dimensional tensile behavior, Res Mechanica 18 (1986) 251–263.
[19] K. Tanaka, S. Kobayashi, Y. Sato, Thermomechanics of transformation pseudoelasticity and shape memory effect in alloys, Int. J. Plasticity 2 (1986) 59–72.